ResearchGate

See discussions, stats, and author profiles for this publication at: https://www.researchgate.net/publication/263983851

Carbon Nanohorn–Porphyrin Dimer Hybrid Material for Enhancing Light-Energy Conversion

ARTICLE *in* THE JOURNAL OF PHYSICAL CHEMISTRY C · APRIL 2012

Impact Factor: 4.77 · DOI: 10.1021/jp302178q

CITATIONS
22

READS
26

8 AUTHORS, INCLUDING:

Georgia Pagona
National Hellenic Research Foundation
44 PUBLICATIONS **725** CITATIONS
SEE PROFILE

Osamu Ito
Tohoku University
593 PUBLICATIONS **15,904** CITATIONS
SEE PROFILE

Georgios Charalambidis
University of Crete
43 PUBLICATIONS **408** CITATIONS
SEE PROFILE

Thanassis Coutsolelos
University of Crete
124 PUBLICATIONS **1,383** CITATIONS
SEE PROFILE

Available from: Thanassis Coutsolelos
Retrieved on: 30 January 2016

THE JOURNAL OF PHYSICAL CHEMISTRY C

Article

pubs.acs.org/JPCC

Carbon Nanohorn–Porphyrin Dimer Hybrid Material for Enhancing Light-Energy Conversion

Georgia Pagona,[†] Galateia E. Zervaki,[‡] Atula S. D. Sandanayaka,[§] Osamu Ito,[∥] Georgios Charalambidis,[‡] Taku Hasobe,*[,⊥] Athanassios G. Coutsolelos,*[,‡] and Nikos Tagmatarchis*[,†]

[†]Theoretical and Physical Chemistry Institute, National Hellenic Research Foundation, 48 Vassileos Constantinou Avenue, Athens 116 35, Greece

[‡]Department of Chemistry, University of Crete, PO Box 2208, Heraklion 710 03, Crete, Greece

[§]School of Materials Science, Japan Advanced Institute of Science and Technology, Asahidai, Nomi, 923-1292, Japan

[∥]CarbonPhotoScience Lab, Kitanakayama 2-1-6, Sendai, 981-3215, Japan

[⊥]Department of Chemistry, Faculty of Science and Technology, Keio University, Yokohama 223-8522, Japan

Supporting Information

ABSTRACT: The covalent grafting through a rigid ester bond of a dimeric porphyrin [$(H_2P)_2$] and carbon nanohorns (CNHs) was accomplished. The newly formed CNH–$(H_2P)_2$ hybrid was found to be soluble or dispersible in several organic solvents. Application of diverse spectroscopic techniques verified the successful formation of the CNH–$(H_2P)_2$ hybrid material. In addition, thermogravimetric analysis revealed the amount of $(H_2P)_2$ loading onto CNHs, and TEM studies showed the characteristic secondary spherical superstructure morphology of the hybrid material. Efficient fluorescence quenching of $(H_2P)_2$ in the CNH–$(H_2P)_2$ hybrid suggests that photoinduced events occur from the photoexcited $(H_2P)_2$ to CNHs. Nanosecond transient absorption spectroscopy revealed the formation of transient species such as $(H_2P)_2^{\bullet+}$ and $CNH^{\bullet-}$ by photoinduced charge separation in CNH–$(H_2P)_2$. Additional proof for the photoinduced charge-separated state $CNH^{\bullet-}$–$(H_2P)_2^{\bullet+}$ was obtained, from which the electron mediates to added hexyl viologen dication (HV^{2+}). Finally, the CNH–$(H_2P)_2$ was adsorbed on nanostructured SnO_2 electrode, to construct a photoactive electrode, which reveals photocurrent and photovoltage responses with an incident photon-to-current conversion efficiency value as large as 9.6%, without the application of any bias voltage.

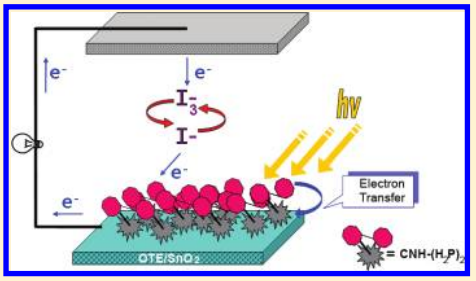

INTRODUCTION

In photovoltaic cells, light is converted to electricity. Considering that photovoltaic processes[1] mimic natural photosynthesis, such as in light harvesting as well as charge separation and transport, diverse strategies have been developed to interface and combine organic electron donors and acceptors into novel hybrid structures. Nowadays, significant research efforts have been given to establish more organized hybrid nanostructures,[2] in which the individual components are tightly bound together via stable and robust covalent bonds. Along these lines, among the most examined and promising electron donors for energy conversion processes are porphyrin dyes, which play a major role in photosynthesis, as they are the skeleton of the chlorophyll present in the photosynthetic reaction center. As key building blocks for artificial photosynthesis, porphyrins contain an extensively conjugated two-dimensional π-system, showing rich and extensive absorption in the visible region with high extinction coefficients, resulting in high light-harvesting capabilities, while they are photostable with tunable redox properties and can be easily prepared.[3,4]

Although quinone derivatives are used as electron acceptors in the reaction center of the natural photosynthesis system, carbon-based nanostructured materials such as fullerenes, nanotubes, and nanohorns can be employed as electron acceptors, combining with porphyrins in model photosynthesis systems,[5] envisioning the next generation of photovoltaics. A plethora of hybrid materials composed of spherical fullerenes and elongated nanotubes covalently combined with porphyrin pigments have been prepared and tested in terms of efficiently managing electron transfer processes;[6,7] however, the field of research with carbon nanohorns (CNHs), prepared by the laser ablation of pure graphite,[8] is not rich, even though they hold the following advantageous parameters: (i) high carbon purity due to the absence of any metal catalyst and impurities during laser ablation production; (ii) heterogeneous surface curvature with highly stretched five-membered rings present at the conical tips, responsible for enhanced reactivity; and (iii) rough secondary spherical superstructure preventing further contact and aggregation, as compared with the other carbon nanomaterials. In addition, pristine CNHs showed semiconducting properties.[9,10]

Received: March 6, 2012
Revised: April 6, 2012
Published: April 6, 2012

 © 2012 American Chemical Society dx.doi.org/10.1021/jp302178q | J. Phys. Chem. C 2012, 116, 9439–9449

In order to build devices constructed of CNHs on substrates, fine dispersions must be obtained. Thus, it is essential to chemically functionalize and solubilize CNHs. Variable strategies became available in the past years, introducing organic addends covalently attached onto the outer surface of CNHs, thus yielding soluble CNH-based materials.[11,12] Moreover, some novel CNH-based hybrid materials, in which the characteristic properties of CNHs are combined with those of Au[13] or CdS[14] nanoparticles as well as photoactive components such as porphyrins,[15] terpyridine,[16] and recently coumarins,[17] have been prepared and have shown that photoillumination induces intrahybrid charge-separation, while some of them have been tested in energy conversion schemes as active components (i.e., photoanodes) in prototype devices.[18] Actually, the efficiencies measured in the latter paradigms examining CNH-based hybrid materials as photovoltaic cells were low, thus giving ample space for designing new materials that may lead to better efficiencies. In fact, (i) when a porphyrin unit was successfully introduced onto CNHs, an efficient intrahybrid charge separation was confirmed,[15b] while an incident photocurrent efficiency (IPCE) value of 2.7%, in the absence of any bias voltage applied, was obtained,[18a] and (ii) when a zinc porphyrin formed an inclusion complex with ammonium-modified CNHs, an IPCE value of 9%, under an applied bias voltage of +0.2 V vs SCE (i.e., meaning that in the absence of any bias voltage the IPCE value should have been considerably smaller), was reached.[18b]

In the present work, the covalent functionalization of CNHs with a dimeric porphyrin as photoexcited electron donor species possessing greater light harvesting as compared with the individual monomer porphyrin is pursued. The aim is to improve the stabilization of the photoinduced charge separated states so that they persist for a longer period of time and to mediate efficiently charges to the electrodes, which would advance the incident photon-to-current conversion efficiency (IPCE). The aspiration of the current research is 3-fold, namely, (i) to succeed in the preparation of a CNH-based hybrid covalently carrying a dimer porphyrin dye, (ii) to assess the photophysical and redox characteristics of that hybrid material, and (iii) to assemble and fabricate the CNH-based hybrid material as an electrode in a photoelectrochemical cell system. The produced nanohybrid material, in which the porphyrin dimer is grafted to the carbon framework of CNHs through a stable and robust covalent bond, is rendered soluble in organic solvents. The latter property allowed us to perform a full spectroscopic characterization study for the new hybrid material; to investigate photoinduced intrahybrid electron transfer mechanisms; to evaluate significant photophysical and electrochemical parameters, such as charge separation and recombination lifetimes and quantum yields, as well as redox potentials and energy levels of the charge separated states; and, most importantly, to construct a prototype photovoltaic device by fabricating the hybrid material as photoanode in a photoelectrochemical cell and to test its efficiency and response.

EXPERIMENTAL SECTION

Electrochemistry. For electrochemistry measurements a standard three-electrode cell was used. Platinum wires were used as counter and working electrodes, while $Ag/AgNO_3$ 0.1 M in acetonitrile was used as a reference electrode. Tetrabutylammonium hexafluorophosphate [$(n\text{-}Bu)_4NPF_6$] (98%) recrystallized three times from acetone and dried in a vacuum at 100 °C was used as the electrolyte. Before each experiment the cell was purged with high purity N_2 for 5 min. Before the start of the measurement the inert gas was turned to "blanket mode". Cyclic voltammetry was recorded by using an EG&G Princeton Applied Research potensiostat/galvanostat model 2273 connected to a personal computer running PowerSuite software. The $Ag/AgNO_3$ electrode was calibrated before each experiment by running cyclic voltammetry on ferrocene.

Fluorescence Lifetime. Picosecond time-resolved fluorescence spectra were measured by using a streakscope (Hamamatsu Photonics, C5680) as a detector and the laser light (Hamamatsu Photonics M10306, laser diode head, 408 nm) as an excitation source.

Nanosecond Transient Absorption. Nanosecond transient absorption measurements were carried out using SHG (532 nm) of a Nd:YAG laser (Spectra-Physics, Quanta-Ray GCR-250-10, 6 ns fwhm) as an excitation source. For transient absorption spectra and the time profiles, monitoring light from a pulsed Xe flash lamp (Hamamatsu Photonics C4479) was detected with a CCD detector equipped with an ICCD-1024G image intensifier (Princeton Instruments). The time profile was analyzed with software supplied with the instrumentation (WinSpec software).

Photoelectrochemical Measurements. Photoelectrochemical measurements were carried out in a standard two-compartment cell consisting of a working electrode and a Pt wire gauze counter electrode. A KEITHLEY 2400 was used for recording I–V characteristics and photocurrent generation density under an AM 1.5 simulated light source (OTENTO-SUN II, Bunkoh Keiki Co., LTD). For the IPCE measurements, a monochromator (SM-25, Bunkoh Keiki Co., Ltd) was introduced into the path of the excitation beam (300 W xenon lamp, Bunkoh Keiki Co., Ltd) for the selection of the wavelength. The lamp intensity at each wavelength was determined using a Si photodiode (Hamamatsu Photonics S1337-1010BQ) and was corrected.

Materials. All solvents and reagents were purchased from Aldrich and used without further purification unless otherwise stated.

Synthesis of 5-[4-(5-(4-Phenoxy)-10,15,20-triphenylporphyrinato)carbonylphenyl]-15-(4-carboxyphenyl)-10,20-bis(2,4,6-trimethylphenyl)porphryin (3). To 5,15-bis(4-carboxyphenyl)-10,20-bis(mesityl)porphyrin (140 mg, 0.178 mmol) in dry dichloromethane (28 mL) was added oxalyl chloride (0.015 mL, 0.178 mmol). The mixture was stirred at 45 °C for 1 h and then the dichloromethane and the oxalyl chloride were removed under reduced pressure. To the resulting solid dissolved in dry THF (10 mL) was added 5-(4-hydroxyphenyl)-10,15,20-triphenylporphyrin (112 mg, 0.178 mmol) in dry THF (13 mL) dropwise over 30 min. Then, an excess of dry triethylamine (1.17 mL, 8.4 mmol) was added for neutralizing the so-produced HCl, and the mixture was stirred at 65 °C overnight. After removal of all volatiles under reduced pressure, the crude solid was submitted to column chromatography (silica gel) with dichloromethane–ethyl acetate (from 100:0 to 95:5) as eluent to afford 62 mg of porphyrin dimer $(H_2P)_2$ **3** in 25% yield. ^1H NMR (300 MHz, $CDCl_3$): δ 9.01 (d, J = 4.8 Hz, 2H), 8.94 (d, J = 4.8 Hz, 2H), 8.89 (m, 6H), 8.81 (m, J = 4.8 Hz, 8H), 8.57 (d, J = 8.1 Hz, 2H), 8.52 (d, J = 8.1 Hz, 2H), 8.41 (m, 4H), 8.26 (m, 6H), 7.80 (m, 11H), 7.34 (s, 4H), 2.67 (s, 6H), 1.91 (s, 12H), −2.55 (s, 2H), −2.71 (s, 2H). ^{13}C NMR (75 MHz, $CDCl_3$): δ 171.4,

Scheme 1. (a) Synthesis of $(H_2P)_2$ 3, (b) Preparation of Ammonium-Functionalized CNH-Based Material 5, and (c) Preparation of CNH−$(H_2P)_2$ Hybrid 6

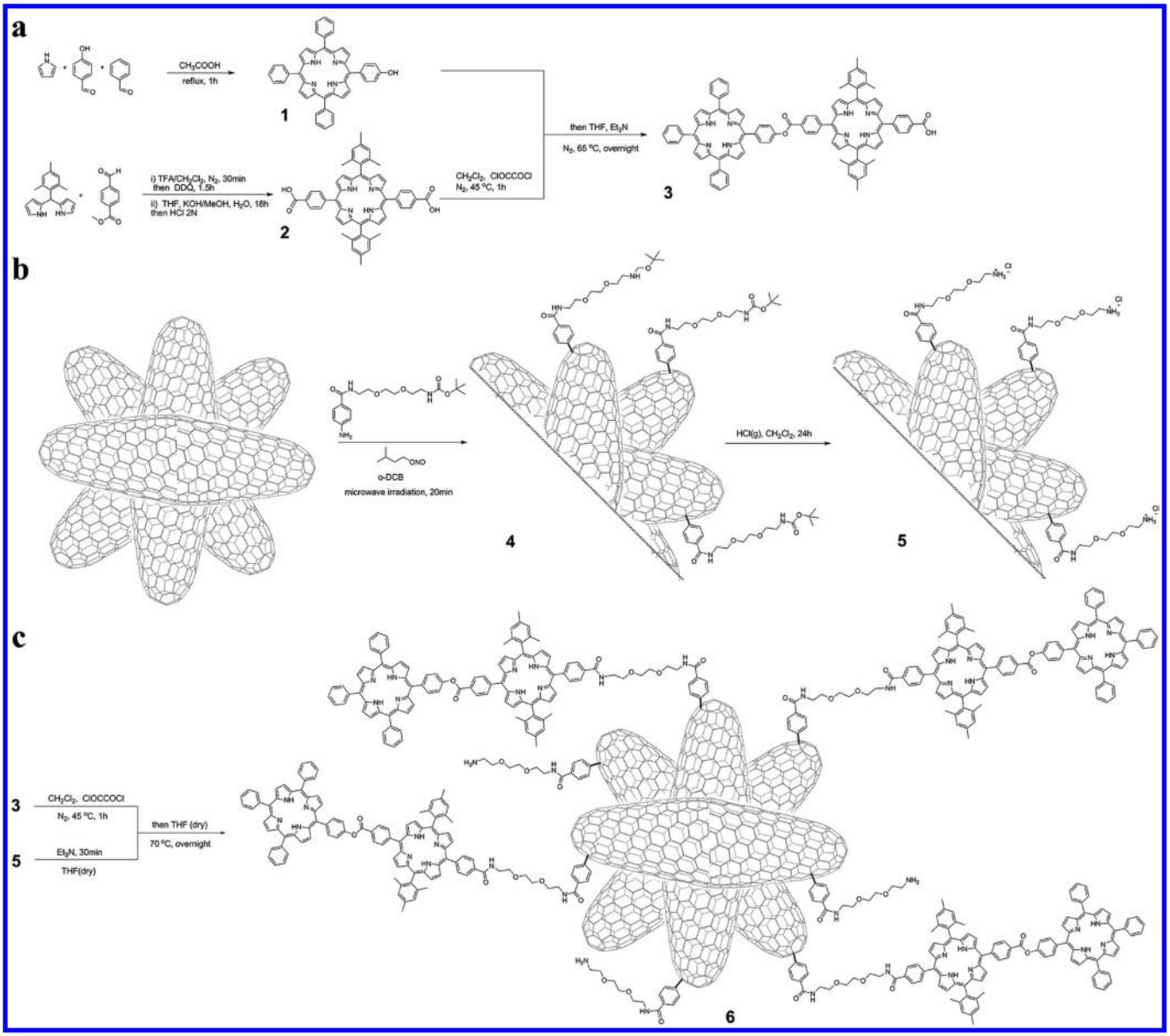

165.8, 151.2, 147.9, 147.9, 142.3, 140.2, 139.5, 138.3, 138.1, 135.7, 135.0, 134.8, 134.7, 131.3, 130.4, 129.2, 128.8, 128.7, 128.0, 127.9, 126.9, 120.5, 120.4, 120.3, 119.2, 119.1, 118.3, 118.2, 21.8, 21.6. HRMS (MALDI-TOF): calcd for $C_{96}H_{70}N_8O_4$ + H^+ 1399.5598 $[M + H]^+$, found 1399.5576. UV−vis, λ/nm ($\varepsilon \times 10^3/M^{-1}$ cm^{-1}): 420 (542.6), 515 (27.3), 550 (12.4), 590 (8.6), 646 (6.5).

Preparation of CNH−$(H_2P)_2$ Hybrid Material (6). In a round-bottom flask, CNH-based material **5** (5 mg) was suspended in dry THF (10 mL) and treated with triethylamine (0.5 mL) for 2 h. After that period, $(H_2P)_2$ **3**, activated in the form of its acyl chloride (2.4 mg, 1.69 μmol) and dissolved in dry THF (2 mL), was added dropwise and the mixture was heated at 70 °C for 18 h. Then, the black residue was filtered through a PTFE membrane filter (0.1 μm) and extensively washed with DMF and THF to obtain CNH−$(H_2P)_2$ hybrid material **6** as black powder.

Electrophoretic Deposition of OTE/SnO_2/CNH−$(H_2P)_2$. Pristine CNHs (1.20 mg) in THF (10 mL) and CNH−$(H_2P)_2$ hybrid material **6** (1.40 mg) in THF (10 mL), respectively, were transferred to a 1 cm cuvette in which two electrodes (viz., OTE/SnO_2 and OTE) were kept at a distance of 6 mm with a Teflon spacer. A dc electric field (~100 V cm^{-1}) was applied for 2 min between these two electrodes using a PowerPac HV (Bio-Rad). The deposition of the OTE/SnO_2/CNH−$(H_2P)_2$ was recognized as a black film.

RESULTS AND DISCUSSION

The synthesis of 5-[4-(5-(4-phenoxy)-10,15,20-triphenylporphyrinato)carbonylphenyl]-15-(4-carboxyphenyl)-10,20-bis(2,4,6-trimethylphenyl)porphryin **3**—abbreviated as $(H_2P)_2$—in which two porphyrin rings are connected through an ester bond at the meso-position, is schematically shown in Scheme 1a. Briefly, a one-pot reaction between pyrrole, benzaldehyde, and 4-hydroxybenzaldehyde generated meso-substituted 5-(4-hydroxyphenyl)-10,15,20-triphenylporphyrin **1**, in a moderate yield after column chromatography.[19] On

dx.doi.org/10.1021/jp302178q | J. Phys. Chem. C 2012, 116, 9439−9449

the other hand, acid-catalyzed reaction of methyl 4-formylbenzoate and 5-mesityldipyrromethane afforded 5,15-bis(4-carboxyphenyl)-10,20-bis(mesityl)porphyrin **2** after basic hydrolysis.[20] At this point it is important to note that the sterically demanding mesityl moiety present as a substituent of the dipyrromethane was deliberately chosen due to its ability to afford trans-meso substituted porphyrins without scrambling, thus avoiding the formation of a complicated mixture of porphyrins.[21] Then, condensation of porphyrin **1** with acyl chloride activated porphyrin **2** yielded dimeric porphyrin $(H_2P)_2$ **3**, possessing a free carboxylic acid group at the meso-position (Scheme 1a). The structure of $(H_2P)_2$ **3** was verified by ^1H and ^{13}C NMR spectroscopy as well as MALDI TOF mass spectrometry (Supporting Information, Figures S1–S3).

On a parallel route, suitably modified CNHs possessing free amine terminal units were prepared according to Scheme 1b. The first step was the preparation of soluble functionalized CNHs material **4** via the methodology of in situ generated aryl diazonium salts,[22] assisted by microwave irradiation,[23] and their addition onto the skeleton of CNHs. Acidic treatment of **4** resulted in CNH-based material **5** possessing, after neutralization, free amino groups suitable for further chemical transformations. In fact, when **5** was subjected to the Kaiser test, 169 μmol of $-NH_2$ loading per gram of CNHs was estimated.

The realization of the targeted CNH$-(H_2P)_2$ hybrid material **6** was achieved by allowing the acyl chloride activated $(H_2P)_2$ **3** to react with the amino-modified CNH-based material **5**, according to Scheme 1c. The produced CNH$-(H_2P)_2$ hybrid **6** was found to be soluble in a variety of organic solvents, including *o*-dichlorobenzene (*o*-DCB), tetrahydrofuran (THF), *N*,*N*-dimethylformamide (DMF), and toluene, forming black solutions stable for several weeks without any precipitation. Solubility values observed for CNH$-(H_2P)_2$ hybrid **6** are in the range of 0.1–0.3 mg/mL, which were estimated by the following technique: A known amount of **6** was dispersed in 40 mL of each examined solvent under sonication, and then, after standing overnight, the residue was filtered and weighted after drying under vacuum overnight.

Characterization. Initially, CNH$-(H_2P)_2$ hybrid **6** was morphologically evaluated by TEM. The TEM images of CNH$-(H_2P)_2$ (Figure 1a) are compared with those of pristine CNHs (Figure 1b), which reveal that the characteristic dahlia-like spherical superstructure of CNHs is retained in the functionalized hybrid **6**. This observation indicates that microwave irradiation during surface modification of CNHs and the covalent attachment of the porphyrin dimer unit $(H_2P)_2$ does not affect or modify the original morphology and secondary spherical superstructure of CNHs aggregates. Moreover, the particle size distribution of CNH$-(H_2P)_2$ hybrid **6** was estimated by dynamic light scattering (DLS) measurements, and the average diameter for hybrid **6** is around 145 nm in DMF solution (Figure 1c). This value is larger than the size measured by TEM (i.e., around 60–80 nm), indicating that aggregation of about three of CNH particles takes place in the solution.[15c]

The amount of porphyrin species covalently anchored onto the surface of CNHs was evaluated by thermogravimetric analysis. Pristine CNHs are thermally stable under nitrogen atmosphere up to at least 800 °C. On the other hand, the TGA graph of ammonium-modified CNH-based material **5** revealed a 17% weight loss, in the temperature range of 200–500 °C (Figure 2), which is attributed to the thermal decomposition of

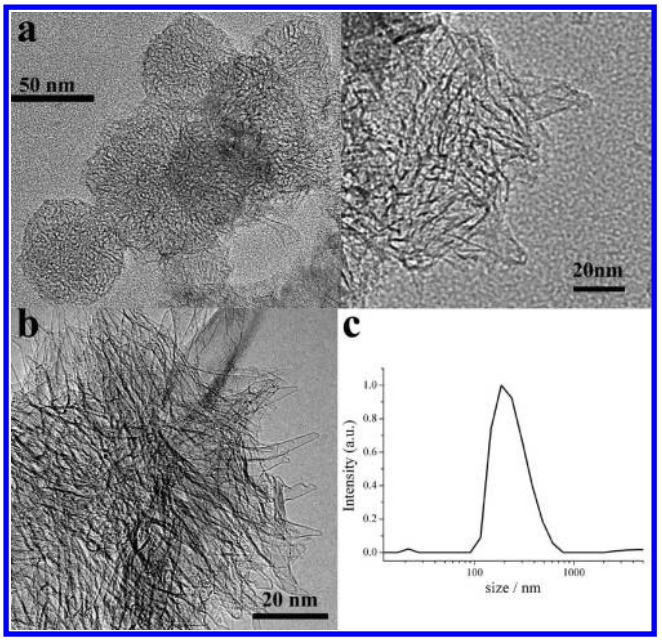

Figure 1. Representative TEM images of (a) CNH$-(H_2P)_2$ hybrid **6** in larger scale (left panel) and smaller scale (right panel) and (b) pristine CNHs. (c) DLS graph of CNH$-(H_2P)_2$ hybrid **6**, obtained in DMF.

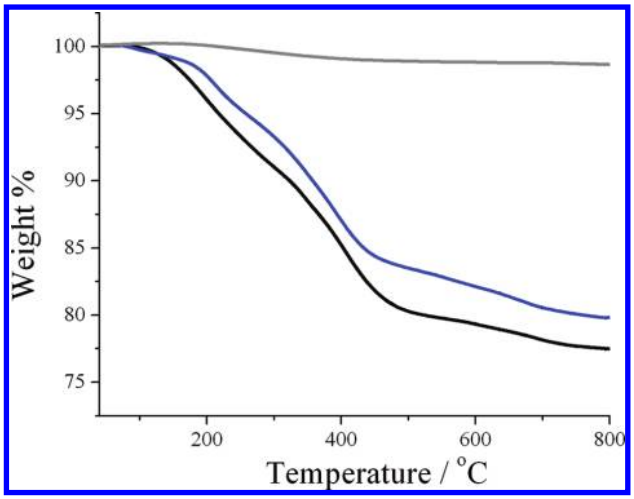

Figure 2. TGA graphs of CNH-based material **5** (blue) and CNH$-(H_2P)_2$ hybrid **6** (black) as compared with pristine CNHs (gray), obtained under nitrogen atmosphere.

the organic units (i.e., aryl units carrying ethylene glycol ammonium ions) attached to nanohorns. Taking this value into account, the number of CNHs carbon atoms per organic moiety is estimated; thus, a functionalization degree of one $-NH_2$ function per every 150 carbon atoms in CNH-based material **5** is given. Then, by combining the above value with the 20% weight loss observed in CNH$-(H_2P)_2$ hybrid material **6** (Figure 2), roughly half of the free $-NH_2$ groups are calculated to be condensed with the porphyrin dimer (see **6** in Scheme 1c), which is reasonably rationalized by considering steric hindrances phenomena introduced by the large volume the dimeric porphyrin is occupying on the surface of CNHs. The weight loss that occurred above 500 °C is attributed to the thermal decomposition of defects created at sites where CNHs functionalization occurred.

dx.doi.org/10.1021/jp302178q | J. Phys. Chem. C 2012, 116, 9439–9449

Spectroscopic insight on the formation of CNH−$(H_2P)_2$ hybrid **6** was delivered by vibrational spectroscopy. In Figure 3,

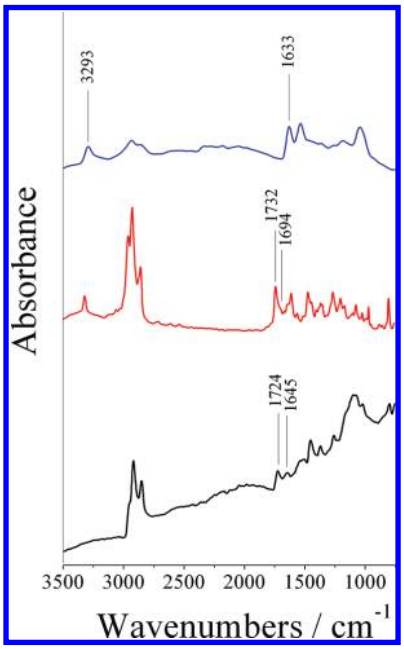

Figure 3. ATR-IR spectra of CNH-based material **5** (blue), $(H_2P)_2$ **3** (red), and CNH−$(H_2P)_2$ hybrid **6** (black).

the ATR-IR spectrum of CNH−$(H_2P)_2$ hybrid **6** is compared with those of porphyrin dimer $(H_2P)_2$ **3** and CNH-based material **5**. The major features in the IR spectrum of porphyrin dimer $(H_2P)_2$ **3** are the carbonyl ester and acid vibrations at 1732 and 1694 cm^{-1}, respectively, and the C−H stretching vibrations at 2968−2857 cm^{-1}. On the other hand, although vibrations at 3293 and 1694 cm^{-1} can be attributed to the ammonium units and carboxylic acid groups in CNH-based material **5** and porphyrin dimer $(H_2P)_2$ **3**, respectively, they are absent in the spectrum of CNH−$(H_2P)_2$ hybrid material **6**. Instead, peaks for CNH−$(H_2P)_2$ at 1645 and 1724 cm^{-1} are observed assignable to the carbonyl amide between $(H_2P)_2$ and CNHs and the ester of the intradimer bond connecting the two porphyrin units, respectively. Furthermore, the strong ATR-IR bands observed at 2960−2852 cm^{-1} are due to the C−H stretching vibrations in CNH−$(H_2P)_2$ hybrid **6**.

Raman spectroscopy was also applied to follow the covalent transformation of CNHs. Basically, the Raman spectrum of pristine CNHs exhibits two bands with almost equal intensity (Figure 4), i.e., the G-band at 1593 cm^{-1} assigned to the sp^2 bonded carbon atoms and the D-band at 1341 cm^{-1} assigned to the conical terminated tips of nanohorns.[24] For functionalized CNH-based material **4** and CNH−$(H_2P)_2$ hybrid **6**, the Raman spectra shown in Figure 4 are normalized at the G-band for clarity. The Raman spectrum of material **4** displays an increased D-band, that is, a D/G ratio of 1.22 was observed, as opposed to a value of 1.05 obtained for intact CNHs. The enhanced intensity of the D-band and higher D/G ratio are indicative of the covalent modification of CNHs skeleton, as resulted in the generation of sp^3 carbon atoms due to the aryl group addition. Notably, the Raman spectrum of CNH−$(H_2P)_2$ hybrid **6** is almost identical to that of CNH-based material **4**, thus implying the absence of further structural perturbation of the nanohorns skeleton upon condensation of the porphyrin dimer in forming the CNH−$(H_2P)_2$ hybrid **6**.

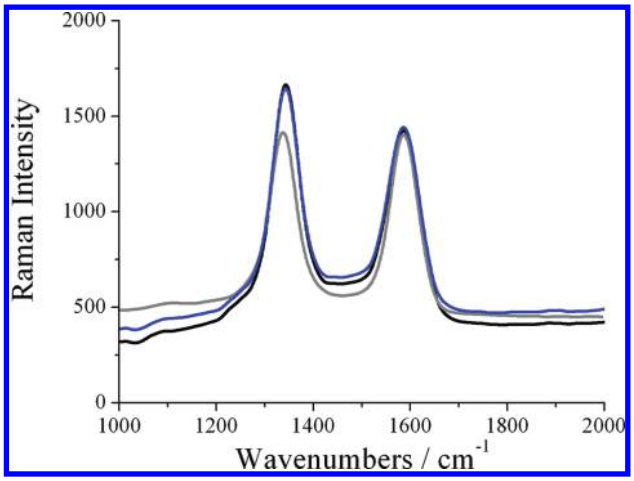

Figure 4. Raman spectra of pristine CNHs (gray) and functionalized CNH-based material **4** (blue) and CNH−$(H_2P)_2$ hybrid **6** (black), obtained at 514 nm excitation wavelength. Spectra are normalized at the G-band for clarity.

Optical Absorption. The electronic absorption spectrum of CNH−$(H_2P)_2$ hybrid **6**, obtained in dichloromethane, is shown in Figure 5. The spectrum exhibits not only a broad

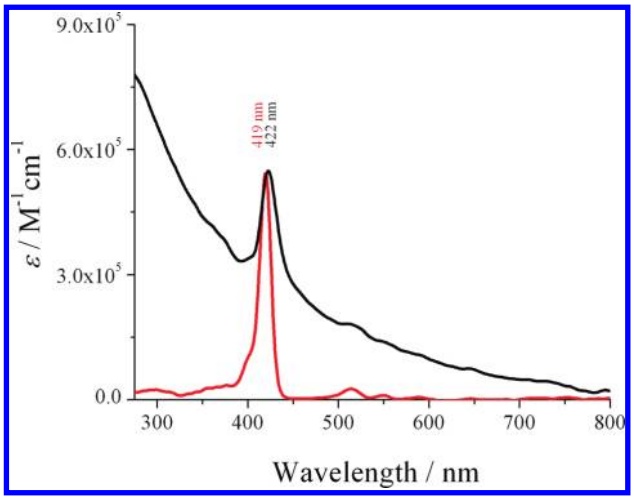

Figure 5. Electronic absorption spectra of free $(H_2P)_2$ **3** (red) and CNH−$(H_2P)_2$ hybrid material **6** (black), obtained in dichloromethane.

band monotonically decreasing from the UV to the visible region, which is typical of CNHs, but also the characteristically strong Soret band at 422 nm, followed by the weak Q-bands at 518, 552, 593, and 649 nm, due to the covalently grafted $(H_2P)_2$ units. Evidently, the $(H_2P)_2$ absorption in **6** is broadened and red-shifted by approximately 3 nm as compared to that of free $(H_2P)_2$ **3** (Figure 5, red spectrum). Such findings based on UV−vis spectroscopy corroborate both the success of the $(H_2P)_2$ linkage to CNHs and ground state electronic interactions between CNHs and $(H_2P)_2$ in hybrid **6**. Such results are in agreement with earlier studies based on other hybrid materials composed of different porphyrins bonded to CNHs in a different fashion.[15,18]

Electrochemistry. The energetics of photoinduced process in CNH−$(H_2P)_2$ hybrid **6** can be evaluated by determining the corresponding redox potentials. Electrochemistry studies of CNH−$(H_2P)_2$ hybrid **6** and free $(H_2P)_2$ **3** were performed by cyclic voltammetry (CV) in dry *o*-DCB:MeCN (5:1), with [(*n*-

dx.doi.org/10.1021/jp302178q | J. Phys. Chem. C 2012, 116, 9439−9449

$Bu)_4NPF_6$] as electrolyte in a standard three-electrode cell with platinum as a working and counter electrode. Evidently, three one-electron reductions and a one-electron oxidation processes were identified in CNH−$(H_2P)_2$ hybrid **6** (Figure 6). The two

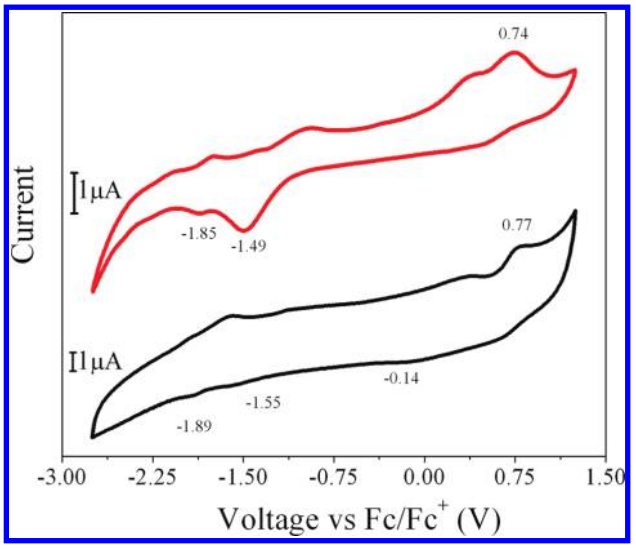

Figure 6. Cyclic voltamograms of CNH−$(H_2P)_2$ hybrid **6** (black) and free $(H_2P)_2$ **3** (red) in *o*-DCB:MeCN 5:1.

reductions and the oxidation refer to the $(H_2P)_2$ unit, while the weak broad signal of the third reduction centered at −0.14 V refers to CNHs.[15−18] The one-electron $(H_2P)_2$ oxidation is observed at 0.77 V, anodically shifted by 30 mV as compared with the oxidation value of unbound $(H_2P)_2$, suggesting appreciable interaction with CNH surfaces. On the other hand, the two one-electron $(H_2P)_2$ reductions observed at −1.89 and −1.55 V were found cathodically shifted by 40 and 60 mV, respectively, as compared with the reduction values of unbound $(H_2P)_2$. From the electrochemical redox data, the driving forces for charge-separation ($-\Delta G_{CS}$) were calculated by employing the Rehm−Weller equation. From the difference between the reduction potential of CNHs (ca. −0.14 V) and the oxidation potential of $(H_2P)_2$ (+0.77 V), the energy level of the charge-separated state can be calculated as ca. 0.91 eV. Therefore, the ΔG_{CS} value via the singlet excited-state of $^1(H_2P)_2$* can be evaluated as −1.0 eV, by employing the energy of $^1(H_2P)_2$* as 1.91 eV obtained from the crossing point of the corresponding absorption and emission spectra (Supporting Information, Figure S4). Overall, the negative value for ΔG_{CS} demonstrates thermodynamically favorable exothermic processes for charge separation from $^1(H_2P)_2$* to CNHs in CNH−$(H_2P)_2$ hybrid **6**, thus forming the radical ion-pair such as $CNH^{\bullet-}$−$(H_2P)_2^{\bullet+}$. All the above redox data and ΔG_{CS} are summarized in Table 1.

Fluorescence Study. To test possible excited state electron donor−acceptor interactions in CNH−$(H_2P)_2$ hybrid **6**, a series of steady-state and time-resolved fluorescence measurements were performed. In more detail, upon photoexcitation at 420 nm in DMF, the strong fluorescence intensities of $(H_2P)_2$ at 650 and 717 nm are significantly quenched in **6**, when measurements are performed with matching absorbencies at the excitation wavelength (Figure 7). In addition, the fluorescence peaks of $(H_2P)_2$ in **6** were found to red-shift by approximately 3 nm as compared with those of free $(H_2P)_2$ **3**. Collectively, these observations are indicative of electronic interactions between

Table 1. Redox Potentials of CNH−$(H_2P)_2$ 6 and $(H_2P)_2$ 3 and Free Energy for Charge Separation[a]

	Redox Potentials vs Fc/Fc^+ (V)				
material	E_{ox}	E^1_{red}	E^2_{red}	E^3_{red}	ΔG_{CS} (eV)
6	0.77	−1.89	−1.55	−0.14[b]	−1.0
3	0.74	−1.85	−1.49		

[a]Measurements were performed using platinum as a working and counter electrode in a 0.1 M $TBAPF_6$ as supporting electrolyte in *o*-DCB:MeCN 5:1 at a rate of 100 mV/s. [b]Broad signal.

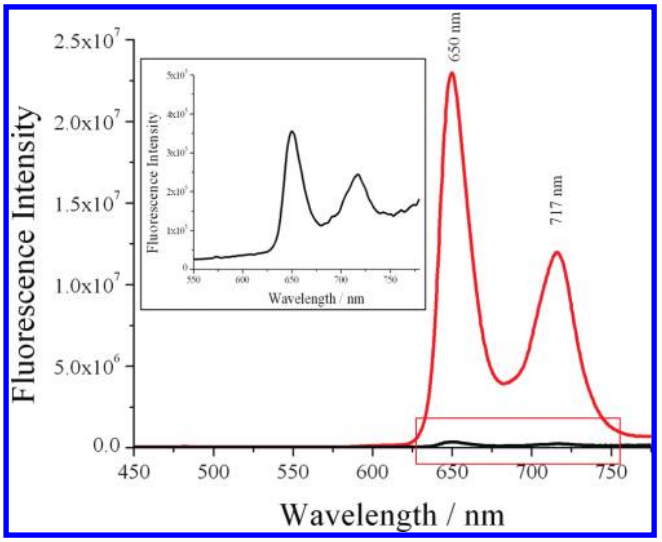

Figure 7. Fluorescence spectra of CNH−$(H_2P)_2$ hybrid **6** (black) as compared with free $(H_2P)_2$ **3** (red), obtained in DMF. The excitation wavelength was 420 nm, and the concentrations were adjusted so that the samples exhibited equal absorbance at the excitation wavelength. Inset: expanded spectrum for CNH−$(H_2P)_2$ hybrid **6**.

the singlet excited state of $(H_2P)_2$, namely, ($^1[(H_2P)_2]$*), and CNHs, suggesting that either electron or energy transfer via $^1[(H_2P)_2]$* to the CNHs unit in **6** occurs. Since, modifying the solvent polarity from polar DMF (dielectric constant ε = 38.3) to less polar CH_2Cl_2 (ε = 9.1) and toluene (ε = 2.4) resulted in gradually lesser fluorescence quenching of the $(H_2P)_2$ moiety for hybrid **6** (Supporting Information, Figure S5), the electron transfer mechanism may be dominant.

In the following step, the photoinduced dynamics of CNH−$(H_2P)_2$ excited states were investigated by following the fluorescence time profiles measurements. Thus, on the basis of the time-correlated single photon counting (TCSPC) method, the fluorescence decay profile for CNH−$(H_2P)_2$ hybrid **6** was obtained upon photoexcitation at 408 nm in CH_2Cl_2, as shown in Figure 8, to which the time profile of reference $(H_2P)_2$ **3** is also shown. The time profile of the fluorescence decay at 650 nm for the singlet excited-state of reference $(H_2P)_2$ **3** was exclusively monoexponentially fitted, with a lifetime of 9400 ps. However, the fluorescence decay of CNH−$(H_2P)_2$ hybrid **6** was curve-fitted by dual-exponential function, from which a fast-decaying component of 460 ps (fraction 85%) and a slower one of 1300 ps (fraction 15%) were evaluated in CH_2Cl_2, as summarized in Table 2. The fast-decaying component of $^1[(H_2P)_2]$* in CNH−$(H_2P)_2$ corresponds to the quenching of the fluorescence intensity in the steady-state spectra (cf. Figure 7). By attributing the fast-decaying component to the charge-separation within hybrid **6**, via $^1[(H_2P)_2]$*, the rate constant for charge separation (k_{CS})

dx.doi.org/10.1021/jp302178q | J. Phys. Chem. C 2012, 116, 9439−9449

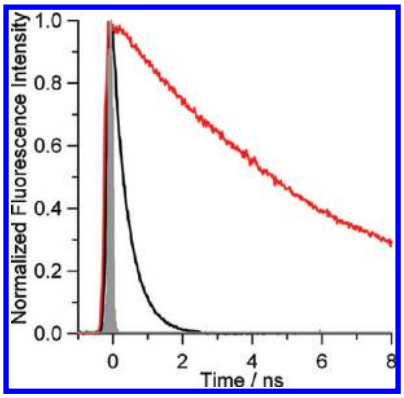

Figure 8. Fluorescence decay profiles of CNH−$(H_2P)_2$ hybrid **6** (black) and free $(H_2P)_2$ **3** (red), obtained in CH_2Cl_2 at 408 nm excitation wavelength; the gray shadow is the laser pulse.

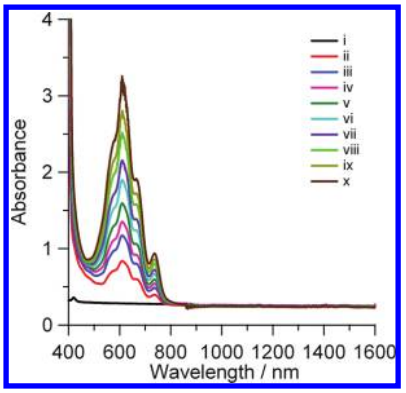

Figure 9. Steady-state absorption spectra of CNH−$(H_2P)_2$ hybrid **6**, obtained in Ar-saturated CH_2Cl_2 solution, measured after five pulsed laser light shots at 532 nm, in the presence of HV^{2+} (0.05 mM) and BNAH: (i) 0, (ii) 0.4, (iii) 0.6, (iv) 0.8, (v) 1.0, (vi) 1.2, (vii) 1.4, (viii) 1.6, (ix) 1.8, and (x) 2.0 mM.

and quantum yield (Φ_{CS}) can be evaluated as 2.1×10^9 s^{-1} and 0.95, respectively. On the other hand, the longer fluorescence lifetime may be assigned to a slow charge-separation process for either a minor component of the hybrid, in which the $(H_2P)_2$ moieties do not have the appropriate conformation and geometry for obtaining higher electronic interactions with CNHs framework, or aggregated $(H_2P)_2$ moieties located in close proximity on CNHs.

Electron Pooling. In the following set of experiments, the charge separation process generating the radical ion pair $CNH^{\bullet-}-(H_2P)_2^{\bullet+}$ was further confirmed, by monitoring steady-state absorption spectral changes upon photoirradiation of nanohybrid **6**, in the presence of an electron-mediating agent such as hexyl viologen (HV^{2+}) and a hole-shift agent such as 1-benzyl-1,4-dihydronicotinamide (BNAH). Thus, as documented in Figure 9, accumulation of $HV^{\bullet+}$ is manifested by growing of the characteristic band at 620 nm, with repeated 532 nm laser excitation of the $(H_2P)_2$ moiety. Notably, when nanohybrid **6** was photoilluminated only in the presence of HV^{2+}, (i.e., in the absence of BNAH), no $HV^{\bullet+}$ was accumulated. These observations support electron mediating from $CNH^{\bullet-}-(H_2P)_2^{\bullet+}$ to HV^{2+}, resulting in electron pooling in solution. Since the $HV^{\bullet+}$concentration increases with increasing amounts of BNAH, the hole on $CNH^{\bullet-}-(H_2P)_2^{\bullet+}$ is transferred to BNAH, forming the closed-shell 1-benzylnicotinamidium ion (BNA^+) possessing a poor electron-accepting ability, thus suggesting that back electron transfer from the electron-rich $HV^{\bullet+}$ to the electron poor $(H_2P)_2^{\bullet+}$ is suppressed.[18b,25]

Nanosecond Transient Absorption. To confirm the electron transfer and to investigate dynamics in CNH−$(H_2P)_2$ hybrid **6**, transient absorption spectroscopy measurements were performed. Upon predominantly excitation of the isolated $(H_2P)_2$ with 532 nm laser light (5 ns pulse, ca. 1 mJ/pulse), the triplet−triplet (T−T) absorption of $(H_2P)_2$ appeared at 440 nm as the main band as well as weak bands at 600 and 700−900 nm (Supporting Information, Figure S6). The lifetime of the triplet state (τ_T) evaluated from the time profile at 440 nm is 12 μs (decay rate $k_T = 8.8 \times 10^4$ s^{-1}), in Ar-saturated dichloromethane solution. On the contrary, upon exciting CNH−$(H_2P)_2$ hybrid **6** by the 532 nm laser light,[26] the main absorption band appeared in the visible region around 600−650 nm, as shown in Figure 10, instead of the T−T absorption bands of $(H_2P)_2$. Thus, the main absorption around 600−650 nm is attributed to the radical cation of $(H_2P)_2^{\bullet+}$.[27] In addition, the broad bands emerging in the NIR region longer than 900 nm, maximizing around 1400 nm, can be ascribed to electrons trapped within the nanohorns (i.e., $CNH^{\bullet-}$), as observed in the previous reports.[15,16,18b] These transient absorption bands support the formation of $CNH^{\bullet-}-(H_2P)_2^{\bullet+}$. The absence of the T−T absorption bands of $(H_2P)_2$ in CNH−$(H_2P)_2$ (Figure 10) suggests that the charge-separation process via $^1[(H_2P)_2]^*$

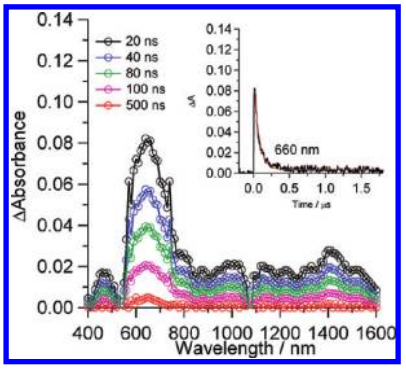

Figure 10. Nanosecond transient absorption spectra of CNH−$(H_2P)_2$ hybrid **6** in Ar-saturated CH_2Cl_2 observed by 532 nm laser light (ca. 1 mJ/pulse). Inset: Absorption−time profiles.

Table 2. Fluorescence Lifetimes, Rate Constant, and Quantum Yield for Charge-Separation and Charge-Recombination in CNH−$(H_2P)_2$ hybrid 6, obtained in CH_2Cl_2

	charge separation				charge recombination	
material	τ_f (ps)[a]		k_{CS} (s^{-1})[b]	Φ_{CS}	τ_{RIP} (ns)[c]	k_{CR} (s^{-1})[d]
6	460 (85%)[e]	1300 (15%)[e]	2.1×10^9	0.95 (0.81)[f]	72	1.4×10^7

[a]Fluorescence lifetime. [b]Charge separation rate constant. [c]Radical ion pair lifetime. [d]Charge recombination rate constant. [e]Fraction of two-component fitting. [f]Φ_{CS} × fraction.

dx.doi.org/10.1021/jp302178q | J. Phys. Chem. C 2012, 116, 9439−9449

becomes predominant to the intersystem crossing to $^3[(H_2P)_2]^*$. After 20 ns, these absorption bands decay monotonously; at 80 ns, the initial intensity decreases by half. The inset of Figure 10 shows the time profile at 660 nm, which exhibits a rapid rise and slow decay within about 200 ns. It is reasonable to attribute the decay of the transient absorption bands to a charge recombination process of $CNH^{\bullet-}-(H_2P)_2^{\bullet+}$. From the first-order fitting of decay time profile at 660 nm, the rate constant of the charge recombination process (k_{CR}) is 1.4 $\times$ 10^7 s^{-1}, which corresponds to the lifetime of $CNH^{\bullet-}-(H_2P)_2^{\bullet+}$ (τ_{RIP}) being 72 ns in CH_2Cl_2. Collectively, all photophysical parameters for $CNH-(H_2P)_2$ hybrid **6** are shown in Table 2.

The electron transfer pathways for $CNH-(H_2P)_2$ hybrid **6** upon photoillumination in the presence of HV^{2+} and BNAH are schematically illustrated in Figure 11. Initially, it is clearly

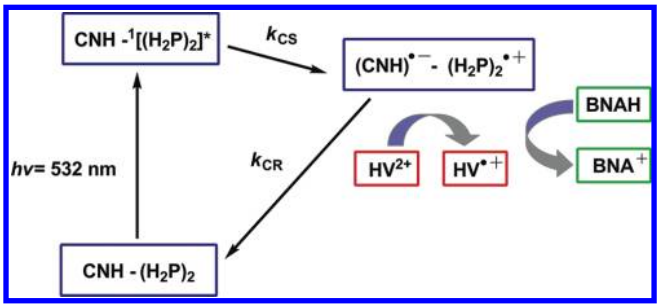

Figure 11. Photoinduced pathways for $CNH-(H_2P)_2$ hybrid **6** upon photoexcitation.

shown that charge separation occurs via $^1(H_2P)_2^*$, thus generating $CNH^{\bullet-}-(H_2P)_2^{\bullet+}$. Evidently, the charge-separation process is exothermic, on the basis of the energies calculated from the energy level of $^1(H_2P)_2^*$ and the one-electron oxidation and reduction of $(H_2P)_2$ and CNHs, respectively. Then, the electron mediation process from $CNH^{\bullet-}$ to added HV^{2+} is slightly endothermic (ca. 0.1 eV) on the comparison of the observed E_{red} value of CNH with that of HV^{2+} (E_{red} = −0.30 V vs Fc/Fc^+). However, this electron-mediating process may be possible under high concentration of HV^{2+}.[28] The electron mediation to HV^{2+} yields $HV^{\bullet+}$, while the hole of $(H_2P)_2^{\bullet+}$ transfers to BNAH, finally yielding BNA^+.[24] Thus, accumulation of $HV^{\bullet+}$ can be reasonably explained by the kinetics.

Device Fabrication. Since the formation and decay of a charge-separated state of $CNH^{\bullet-}-(H_2P)_2^{\bullet+}$ and its electron mediating have been established, we constructed a photoelectrochemical cell employing $CNH-(H_2P)_2$ hybrid **6** as an active electrode. Notably, as the rate constant for charge separation is larger than that for charge recombination by two orders in $CNH-(H_2P)_2$ hybrid **6**, it is quite feasible to extract the separated charges, electrons, and holes, incorporating **6** into a photovoltaic cell. To construct such a cell, electrophoretic deposition was applied to fabricate films of $CNH-(H_2P)_2$ hybrid **6** onto nanostructured SnO_2 films on an optically transparent electrode (OTE).[18] The process for the fabrication is briefly described as follows. A suspension of $CNH-(H_2P)_2$ hybrid **6** in THF (~2 mL) was transferred into a cuvette, in which an OTE and the OTE/SnO_2 electrodes were inserted and kept at some distance with the aid of a Teflon spacer. Then, by applying dc electric field (~100 V/cm) between the two electrodes, the $CNH-(H_2P)_2$ hybrid **6** from the suspension was driven to the electrode surface, and a robust thin film of $OTE/SnO_2/CNH-(H_2P)_2$ was shortly deposited. Analogously, $OTE/SnO_2/CNHs$ and $OTE/SnO_2/(H_2P)_2$ were prepared. In the steady-state absorption spectra of $OTE/SnO_2/CNH-(H_2P)_2$ (Supporting Information, Figure S7), the main band observed is related with the Soret band of the $(H_2P)_2$. However, further broadening of the absorption bands was observed for $OTE/SnO_2/CNH-(H_2P)_2$ as compared with the corresponding band of $CNH-(H_2P)_2$ hybrid material **6** in solution (cf. Figure 5), suggesting the clustering of $CNH-(H_2P)_2$ on OTE/SnO_2.[28,29] The $OTE/SnO_2/CNH$ electrode shows continuous featureless absorbance in the visible region due to the presence of CNHs.

Photocurrent Measurements. Photoelectrochemical measurements were performed in a standard two-compartment cell, in acetonitrile containing 0.5 M LiI and 0.01 M I_2 as redox electrolyte and $OTE/SnO_2/CNH-(H_2P)_2$ as working electrode, while Pt wire was the counter electrode.[18,29] The photocurrent and photovoltage responses of $OTE/SnO_2/CNH-(H_2P)_2$ electrode obtained under white light illumination (AM 1.5 condition; input power 100 mW cm^{-2}) are shown in Figure 12. Evidently, the responses were found to be prompt,

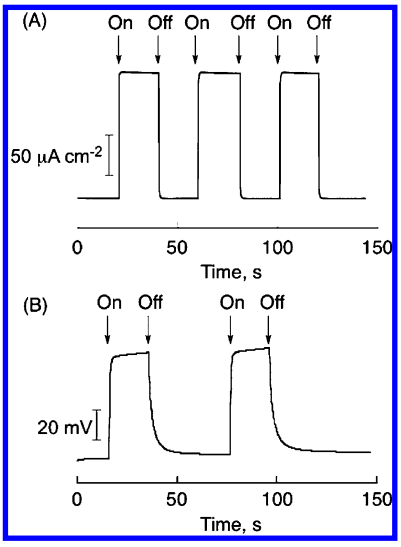

Figure 12. (A) Short circuit photocurrent (I_{sc}) generation response of $OTE/SnO_2/CNH-(H_2P)_2$. (B) Photovoltage response of $OTE/SnO_2/CNH-(H_2P)_2$. Measurements were performed under white light illumination using an AM 1.5 filter, with input power of 100 mW cm^{-2}.

steady, and reproducible during repeated on/off cycles of the visible light illumination. In Figure 12A, the short circuit photocurrent density (I_{sc}) of $OTE/SnO_2/CNH-(H_2P)_2$ was found to be almost 140 μA cm^{-2}, while blank experiments conducted with pristine OTE/SnO_2 produced no detectable photocurrent under similar experimental conditions.[18a,30] Thus, the observation of anodic photocurrent for $OTE/SnO_2/CNH-(H_2P)_2$ films suggests electron transfer from the photoexcited $(H_2P)_2$ to CNHs, followed by OTE/SnO_2. Figure 12B shows that the buildup of ca. 60 mV of photovoltage is considered rather fast, while it attains a steady state under light illumination. Furthermore, it is reproducible during repeated on/off cycles. Overall, the photocurrent and photovoltage responses of $OTE/SnO_2/CNH-(H_2P)_2$ electrode highlight the significance of photo-excited-state dynamic interactions be-

dx.doi.org/10.1021/jp302178q | J. Phys. Chem. C 2012, 116, 9439−9449

tween $(H_2P)_2$ and CNHs in generating a photoelectrochemical effect.

Finally, the photocurrent action spectra were evaluated by examining the wavelength dependence of the incident photon-to-current conversion efficiency (IPCE) by using a standard two-compartment cell equipped with a potentionstat.[31] As shown in Figure 13, the photocurrent action spectra of OTE/SnO_2/CNH−$(H_2P)_2$ and OTE/SnO_2/$(H_2P)_2$ electrodes are similar to the absorption spectra of $(H_2P)_2$. Indeed, the wavelength showing the maximal IPCE value at 420−430 nm corresponds to the absorption peak position of $(H_2P)_2$. The maximal IPCE value of 9.6% at 430 nm was observed for OTE/SnO_2/CNH−$(H_2P)_2$, whereas that for OTE/SnO_2/$(H_2P)_2$ was significantly smaller (3.9% at 430). An even lower IPCE value, that of 1.7% without a peak, was observed for OTE/SnO_2/CNH. These results suggest that the process responsible for the photocurrent generation includes electron-transfer from $^1[(H_2P)_2]^*$ to CNHs, followed by electron mediation from the reduced nanohorns to the conduction band of the SnO_2 electrode.[32] Here it is worth mentioning that the previously reported hybrid material of covalently functionalized CNHs with monomeric porphyrin, namely CNH−H_2P,[15b] showed an IPCE value of only 2.7%.[18a] Thus, the dimeric porphyrin $(H_2P)_2$ covalently grafted onto CNHs, as shown in the present study, has an enhancing effect on the IPCE value. As for such enhancement, the following two factors may be crucial: (i) the higher molar absorption of dimeric porphyrin as compared with the monomeric one [i.e., ε = 542.6 × 10^3 M^{-1} cm^{-1} for the Soret band of $(H_2P)_2$ vs ε = 343.8 × 10^3 M^{-1} cm^{-1} for the Soret band of H_2P][33] and (ii) the higher loading of porphyrin units onto CNHs [i.e., TGA data calculate the loading of one $(H_2P)_2$ unit per 300 carbons vs 400 carbons for the case of monomeric H_2P units[15b]]. Notably, the 9.6% IPCE value obtained without applying any bias potential for OTE/SnO_2/CNH−$(H_2P)_2$ is the highest value ever recorded for donor−acceptor hybrid systems utilizing CNHs.[18,34]

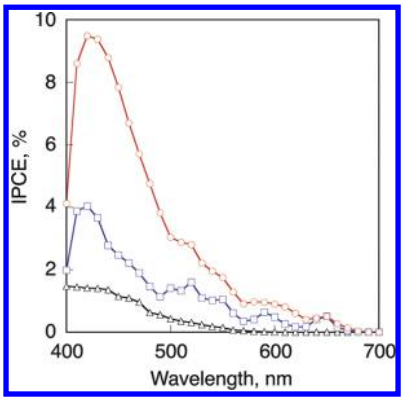

Figure 13. Photocurrent action spectra of OTE/SnO_2/CNH−$(H_2P)_2$ (red), OTE/SnO_2/$(H_2P)_2$ (blue), and OTE/SnO_2/CNH (black), under a standard two-compartment cell. Electrolyte: 0.5 M LiI and I_2 0.01 M in acetonitrile.

CONCLUSION

Dimeric porphyrin $(H_2P)_2$ has been conjugated onto covalently functionalized CNHs, forming electron donor−acceptor CNH−$(H_2P)_2$ hybrid **6**. The new hybrid material was thoroughly characterized with the aid of standard analytical techniques. Steady-state fluorescence measurements revealed efficient quenching of the $(H_2P)_2$ fluorescence in the CNH−$(H_2P)_2$ hybrid, suggesting photoinduced charge-separation via the singlet excited state of $(H_2P)_2$. The energetics of deactivation in CNH−$(H_2P)_2$ as evaluated by redox potentials support the charge-separation. Transient absorption spectroscopy revealed generation of $CNH^{\bullet-}$−$(H_2P)_2^{\bullet+}$. Indirect proof for the photoinduced charge-separation in CNH−$(H_2P)_2$ was derived from the reduction of hexyl viologen dication (HV^{2+}) accumulating monocation radical of $HV^{\bullet+}$. Finally, a photoelectrochemical cell was constructed on the basis of CNH−$(H_2P)_2$ loading onto nanostructured SnO_2 at an optical transparent electrode (OTE). The OTE/SnO_2/CNH−$(H_2P)_2$ electrode revealed prompt, stable, and reproducible photocurrent and photovoltage, with an IPCE value as large as 9.6%, without the application of bias voltage, which is the highest observed among two-compartment cells for CNH-based hybrid materials as well as among other carbon nanostructured materials. The high loading of the electron donor component conjugated onto CNHs and its high molar absorptivity are key factors toward enhancing and improving photoinduced electron transfer efficiency in CNH-based hybrid materials.

ASSOCIATED CONTENT

Supporting Information

Experimental details, spectra of $(H_2P)_2$, absorption and emission spectra of CNH−$(H_2P)_2$, and absorption spectra of OTE/SnO_2/CNH−$(H_2P)_2$ and OTE/SnO_2/CNH films. This material is available free of charge via the Internet at http://pubs.acs.org

AUTHOR INFORMATION

Corresponding Author

*N.T.: tel, + 30 210 7273835; fax, + 30 210 7273794; e-mail, tagmatar@eie.gr. A.G.C.: tel, + 30 2810 545045; fax, + 30 2810 545161; e-mail, coutsole@chemistry.uoc.gr. T.H.: tel, + 81 45 566 1806; fax, + 81 45 566 1197; e-mail: hasobe@chem.keio.ac.jp.

Notes

The authors declare no competing financial interest.

ACKNOWLEDGMENTS

We are deeply indebted to Prof. S. Iijima and Dr. M. Yudasaka for supplying CNHs of the highest quality as well as the productive collaboration and stimulating discussions. Partial financial support from the EU FP7, Capacities Program, NANOHOST project (GA 201729), GSRT/NSRF 2007-2013 Cooperation Action through project 09ΣΥΝ-42-691, and COST network MP0901 NanoTP to N.T. are acknowledged. The European Commission funded this research by FP7-REGPOT-2008-1, Project BIOSOLENUTI No. 229927 (A.G.C). This work was partially supported by Herakleitos II University of Crete Operational Programme of "Education and Lifelong Learning 2007-2013" (E.P.E.D.V.M.) of ESPA (2007-2013), which is funded by the European Union (European Social Fund) and National resources. This work was also partially supported by Grant-in-Aids for Scientific Research (No. 23108721 and 23681025 to T.H.) and the MEXT (The Ministry of Education, Culture, Sports, Science and Technology, Japan)-Supported Program for the Strategic Research Foundation at Private Universities, 2009-2013.0.

REFERENCES

(1) (a) Sun, S. S.; Sariciftci, N. S. In *Organic Photovoltaics*; Taylor & Francis: Boca Raton, FL, 2005. (b) Special issue on "Artificial Photosynthesis and Solar Fuels" *Acc. Chem. Res.* **2009**, *42*, 1859−2029.

(2) (a) Tseng, R. J.; Chan, R.; Tung, V. C.; Yang, Y. *Adv. Mater.* **2008**, *20*, 435−438. (b) Hiramoto, M.; Yamaga, T.; Danno, M.; Suemori, K.; Matsumura, Y.; Yokoyama, M. *Appl. Phys. Lett.* **2006**, *88*, 213105.

(3) Fukuzumi, S. In *The Porphyrin Handbook*; Kadish, K. M., Smith, K. M., Guilard, R., Eds.; Academic Press: San Diego, CA, 2010; Vol. *10*, pp 183−244.

(4) (a) Aratani, N.; Kim, D.; Osuka, A. *Acc. Chem. Res.* **2009**, *42*, 1922−1934. (b) Li, W.-S.; Aida, T. *Chem. Rev.* **2009**, *109*, 6047−6076. (c) Gust, D.; Moore, T. A.; Moore, A. L. *Acc. Chem. Res.* **2009**, *42*, 1890−1898. (d) Imahori, H.; Umeyama, T.; Ito, S. *Acc. Chem. Res.* **2009**, *42*, 1809−1818.

(5) (a) Gust, D.; Moore, T. A.; Moore, A. L. *Acc. Chem. Res.* **2009**, *42*, 1890−1898. (b) Grimm, B.; Hausmann, A.; Kahnt, A.; Seitz, W.; Spanig, F.; Guldi, D. M. In *The Porphyrin Handbook*; Kadish, K. M., Smith, K. M., Guilard, R., Eds.; Academic Press: San Diego, CA, 2010; Vol. *1*, pp 133−220. (c) D'Souza, F.; Sandanayaka, A. S. D.; Ito, O. *J. Phys. Chem. Lett.* **2010**, *1*, 2586−2593. (d) Hasobe, T. *Phys. Chem. Chem. Phys.* **2010**, *12*, 44−57.

(6) For porphyrins covalently attached to fullerenes, see: (a) Oswald, F.; Shafiqul Islam, D.-M.; Araki, Y.; Troiani, V.; Caballero, R.; de la Cruz, P.; Ito, O.; Langa, F. *Chem. Commun.* **2007**, 4498−4500. (b) Winters, M. U.; Dahlstedt, E.; Blades, H. E.; Wilson, C. J.; Frampton, M. J.; Anderson, H. L.; Albinsson, B. *J. Am. Chem. Soc.* **2007**, *129*, 4291−4297. (c) Schumacher, A. L.; Sandanayaka, A. S. D.; Hill, J. P.; Ariga, K.; Karr, P. A.; Araki, Y.; Ito, O.; D'Souza, F. *Chem.—Eur. J.* **2007**, *13*, 4628−4635. (d) D'Souza, F.; Gadde, S.; Schumacher, A. L.; Zandler, M. E.; Sandanayaka, A. S. D.; Araki, Y.; Ito, O. *J. Phys. Chem. C* **2007**, *111*, 11123−11130. (e) Fazio, M. A.; Lee, O. P.; Schuster, D. I. *Org. Lett.* **2008**, *10*, 4979−4982. (f) Fazio, M. A.; Durandin, A.; Tkachenko, N.; Niemi, M.; Lemmetyinen, H.; Schuster, D. I. *Chem.—Eur. J.* **2009**, *15*, 7698−7705. (g) Spanig, F.; Ruppert, M.; Dannhauser, J.; Hirsch, A.; Guldi, D. M. *J. Am. Chem. Soc.* **2009**, *131*, 9378−9388. (h) Schlundt, S.; Kuzmanich, G.; Spanig, S.; Rojas, G. M.; Kovacs, C.; Garcia-Garibay, M. A.; Guldi, D. M.; Hirsch, A. *Chem.—Eur. J.* **2009**, *15*, 12223−12233. (i) Lembo, A.; Tagliatesta, P.; Guldi, D. M.; Wielopolski, M.; Nuccetelli, M. *J. Phys. Chem. A* **2009**, *113*, 1779−1793. (j) Wielopolski, M.; Rojas, G. M.; van der Pol, C.; Brinkhaus, L.; Katsukis, G.; Bryce, M. R.; Clark, T.; Guldi, D. M. *ACS Nano* **2011**, *4*, 6449−6462. (k) Molina-Ontoria, A.; Wielopolski, M.; Gebhardt, J.; Gouloumis, A.; Clark, T.; Guldi, D. M.; Martin, N. *J. Am. Chem. Soc.* **2011**, *133*, 2370−2373. (l) Villegas, C.; Delgado, J. L.; Bouit, P.-A.; Grimm, B.; Seitz, W.; Martin, N.; Guldi, D. M. *Chem. Sci.* **2011**, *2*, 1677−1681. (m) Feng, L.; Slanina, Z.; Sato, S.; Yoza, K.; Tsuchiya, T.; Mizorogi, N.; Akasaka, T.; Nagase, S.; Martin, N.; Guldi, D. M. *Angew. Chem., Int. Ed.* **2011**, *50*, 5909−5912. (n) Iehl, J.; Vartanian, M.; Holler, M.; Nierengarten, J.-F.; Delavaux-Nicot, B.; Strub, J.-M.; Van Dorsselaer, A.; Wu, Y.; Mohanraj, J.; Yoosaf, K.; et al. *J. Mater. Chem.* **2011**, *21*, 1562−1573.

(7) For porphyrins covalently attached to carbon nanotubes, see: (a) Li, H.; Martin, R. B.; Harruff, B. A.; Carino, R. A.; Sun, Y. P. *Adv. Mater.* **2004**, *16*, 896−900. (b) Baskaran, B.; Mays, J. W.; Zhang, X. P.; Bratcher, M. S. *J. Am. Chem. Soc.* **2005**, *127*, 6916−6917. (c) Campidelli, S.; Sooambar, C.; Lozano-Diz, E.; Ehli, C.; Guldi, D. M.; Prato, M. *J. Am. Chem. Soc.* **2006**, *128*, 12544−12552. (d) Guo, Z.; Du, F.; Chen, Y.; Zheng, J.; Liu, Z.; Tian, J. *J. Mater. Chem.* **2006**, *16*, 3021−3030. (e) Ballesteros, B.; de La Torre, G.; Ehli, C.; Aminur-Rahman, G. M.; Agullo-Rueda, F.; Guldi, D. M.; Torres, T. *J. Am. Chem. Soc.* **2007**, *129*, 5061−5068. (f) Palacin, T.; Khanh, H. L.; Jousselme, B.; Jegou, P.; Filoramo, A.; Ehli, C.; Guldi, D. M.; Campidelli, S. *J. Am. Chem. Soc.* **2009**, *131*, 15394−15402. (g) Arai, T.; Nobukuni, S.; Sandanayaka, A. S. D.; Ito, O. *J. Phys. Chem. C* **2009**, *113*, 14493−14499.

(8) Iijima, S.; Yudasaka, M.; Yamada, R.; Bandow, S.; Suenega, K.; Kokai, F.; Takahashi, K. *Chem. Phys. Lett.* **1999**, *309*, 165−170.

(9) Urita, K.; Seki, S.; Utsumi, S.; Noguchi, D.; Kanoh, H.; Tanaka, H.; Hattori, Y.; Ochiai, Y.; Aoki, N.; Yudasaka, M.; et al. *Nano Lett.* **2006**, *6*, 1325−1328.

(10) Zahab, A.; Spina, L.; Poncharal, P.; Marliere, C. *Phys. Rev. B: Condens. Matter Mater. Phys.* **2000**, *62*, 10000−10003.

(11) (a) Tagmatarchis, N.; Maigne, A.; Yudasaka, M.; Iijima, S. *Small* **2006**, *2*, 490−494. (b) Pagona, G.; Fan, J.; Tagmatarchis, N.; Yudasaka, M.; Iijima, S. *Chem. Mater.* **2006**, *18*, 3918−3920. (c) Cioffi, C.; Campidelli, S.; Brunetti, F. G.; Meneghetti, M.; Prato, M. *Chem. Commun.* **2006**, 2129−2131. (d) Pagona, G.; Karousis, N.; Tagmatarchis, N. *Carbon* **2008**, *46*, 604−610. (e) Economopoulos, S. P.; Pagona, G.; Yudasaka, M.; Iijima, S.; Tagmatarchis, N. *J. Mater. Chem.* **2009**, *19*, 7326−7331. (f) Karousis, N.; Ichihashi, T.; Yudasaka, M.; Iijima, S.; Tagmatarchis, N. *Chem. Commun.* **2011**, *47*, 1604−1606.

(12) (a) Pagona, G.; Mountrichas, G.; Rotas, G.; Karousis, N.; Pispas, S.; Tagmatarchis, N. *Int. J. Nanotechnol.* **2009**, *6*, 176−195. (b) Shu, Z.; Xu, G. *Nanoscale* **2010**, *2*, 2538−2549. (c) Yudasaka, M.; Iijima, S. In *Carbon Nanotubes and Related Structures*; Guldi, D. M., Martin, N., Eds., Wiley-VCH Verlag GmbH & Co. KGaA, Weinheim, Germany, 2010; Chapter 13, pp385−404.

(13) (a) Mountrichas, G.; Ichihashi, T.; Pispas, S.; Yudasaka, M.; Iijima, S.; Tagmatarchis, N. *J. Phys. Chem. C* **2009**, *113*, 5444−5449. (b) Karousis, N.; Ichihashi, T.; Chen, S.; Shinohara, H.; Yudasaka, M.; Iijima, S.; Tagmatarchis, N. *J. Mater. Chem.* **2010**, *20*, 2959−2964.

(14) Mountrichas, G.; Pispas, S.; Tagmatarchis, N. *Small* **2007**, *3*, 404−407.

(15) (a) Cioffi, C.; Campidelli, S.; Sooambar, C.; Marcaccio, M.; Marcolongo, G.; Meneghetti, M.; Paolucci, D.; Paolucci, F.; Ehli, C.; Rahman, G. M. A.; et al. *J. Am. Chem. Soc.* **2007**, *129*, 3938−3945. (b) Pagona, G.; Sandanayaka, A. S. D.; Araki, Y.; Fan, J.; Tagmatarchis, N.; Charalambidis, G.; Coutsolelos, A. G.; Boitrel, B.; Yudasaka, M.; Iijima, S.; et al. *Adv. Funct. Mater.* **2007**, *17*, 1705−1711. (c) Sandanayaka, A. S. D.; Ito, O.; Tanaka, T.; Isobe, H.; Nakamura, E.; Yudasaka, M.; Iijima, S. *New. J. Chem.* **2009**, *33*, 2261−2266.

(16) Rotas, G.; Sandanayaka, A. S. D.; Tagmatarchis, N.; Ichihashi, T.; Yudasaka, M.; Iijima, S.; Ito, O. *J. Am. Chem. Soc.* **2008**, *130*, 4725−4731.

(17) Pagona, G.; Katerinopoulos, H. E.; Tagmatarchis, N. *Chem. Phys. Lett.* **2011**, *516*, 76−81.

(18) (a) Pagona, G.; Sandanayaka, A. S. D.; Hasobe, T.; Charalambidis, G.; Coutsolelos, A. G.; Yudasaka, M.; Iijima, S.; Tagmatarchis, N. *J. Phys. Chem. C* **2008**, *112*, 15735−15741. (b) Vizuete, M.; Gomez-Escalonilla, M. J.; Fierro, J. L. G.; Sandanayaka, A. S. D.; Hasobe, T.; Yudasaka, M.; Iijima, S.; Ito, O.; Langa, F. *Chem.—Eur. J.* **2010**, *16*, 10752−10763.

(19) (a) Zhang, W.; Shaikh, A.; Tsui, E. Y.; Swager, T. M. *Chem. Mater.* **2009**, *21*, 3234−3241. (b) Tome, J.; Neves, M.; Tome, A.; Cavaleiro, J.; Mendonca, A.; Pegado, I.; Duarte, R.; Valdeira, M. *Bioorg. Med. Chem.* **2005**, *13*, 3878−3888.

(20) Garcia, G.; Sarrazy, V.; Sol, V.; Le Morvan, C.; Granet, R.; Alves, S.; Krausz, P. *Bioorg. Med. Chem.* **2009**, *117*, 767−776.

(21) (a) Littler, B. J.; Ciringh, Y.; Lindsey, J. S. *J. Org. Chem.* **1999**, *64*, 2864−2872. (b) Rao, P. D.; Dhanalekshmi, S.; Littler, B. J.; Lindsey, J. S. *J. Org. Chem.* **2000**, *65*, 7323−7344.

(22) (a) Bahr, J. L.; Tour, J. M. *Chem. Mater.* **2001**, *13*, 3823−3824. (b) Dyke, C. A.; Tour, J. M. *J. Phys. Chem. A* **2004**, *108*, 11151−11159.

(23) (a) Vazquez, E.; Prato, M. *ACS Nano* **2009**, *3*, 3819−3824. (b) Economopoulos, S. P.; Karousis, N.; Rotas, G.; Pagona, G.; Tagmatarchis, N. *Curr. Org. Chem.* **2011**, *15*, 1121−1132.

(24) Utsumi, S.; Honda, H.; Hattori, Y.; Kanoh, H.; Takahashi, K.; Sakai, H.; Abe, M.; Yudasaka, M.; Iijima, S.; Kaneko, K. *J. Phys. Chem. C* **2007**, *111*, 5572−5575.

(25) (a) Fukuzumi, S.; Koumitsu, S.; Hironaka, K.; Tanaka, T. *J. Am. Chem. Soc.* **1987**, *109*, 305−316. (b) Fukuzumi, S.; Imahori, H.; Okamoto, K.; Yamada, H.; Fujitsuka, M.; Ito, O.; Guldi, D. M. *J. Phys. Chem. A* **2002**, *106*, 1903−1908. (c) Sandanayaka, A. S. D.; Pagona,

G.; Tagmatarchis, N.; Yudasaka, M.; Iijima, S.; Araki, Y.; Ito, O. *J. Mater. Chem.* **2007**, *17*, 2540−2546.
(26) The 532-nm laser light excites the shorter wavelength side of the Q-band of $(H_2P)_2$. Since the broad absorption of CNHs in the visible region is overlapping, it is difficult to evaluate the excited $(H_2P)_2$ molecules quantitatively in the CNH−$(H_2P)_2$ hybrid material **6**.
(27) (a) Imahori, H.; Tamaki, K.; Araki, Y.; Sekiguchi, Y.; Ito, O.; Sakata, Y.; Fukuzumi, S. *J. Am. Chem. Soc.* **2002**, *124*, 5165−5174.
(28) From the slightly endothermic electron transfer (ca. −0.15 eV), the second-order electron-mediating rate constant must be 10^8 M^{-1} s^{-1}; thus, the pseudo-first-order rate constate under higher concentration of HV^{2+} (>0.1 mM) competes with the charge recombiation rate of $CNH^{\bullet-}$−$(H_2P)_2^{\bullet+}$.
(29) Hasobe, T.; Imahori, H.; Fukuzumi, S.; Kamat, P. V. *J. Phys. Chem. B* **2003**, *107*, 12105−12112.
(30) (a) Kongkanand, A.; Tvrdy, K.; Takechi, K.; Kuno, M.; Kamat, P. V. *J. Am. Chem. Soc.* **2008**, *130*, 4007−4015. (b) Kamat, P. V. *J. Phys. Chem. C* **2008**, *112*, 18737−18753. (c) Lee, H. J.; Yum, J. H.; Leventis, H. C.; Zakeeruddin, S. M.; Haque, S. A.; Chen, P.; Seok, S. I.; Graetzel, M.; Nazeeruddin, M. K. *J. Phys. Chem. C* **2008**, *112*, 11600−11608.
(31) IPCE (%) = 100 × 1240 × $I_{sc}/(W_{in}\lambda)$, where I_{sc} is the short circuit photocurrent (A/cm^2), W_{in} is the incident light intensity (W/cm^2), and λ is the wavelength in nm.
(32) The reduction potential of CNHs is rather low; thus, the electron mediation from reduced nanohorns to SnO_2 may eventually be an endothermic process.
(33) Halime, Z.; Lachkar, M.; Matsouki, N.; Charalambidis, G.; di Vaira, M.; Coutsolelos, A. G.; Boitrel, B. *Tetrahedron* **2006**, *62*, 3056−3064.
(34) It was difficult to control the amount of porphyrins and CNHs by the electrophoretic method when depositing molecular assemblies onto the OTE/SnO_2 surface. Therefore, precise comparison of IPCE values between **3** and **5** is difficult to perform.